

A Novel Insular/Orbital-Prelimbic Circuit That Prevents Persistent Avoidance in a Rodent Model of Compulsive Behavior

Freddyson J. Martínez-Rivera, José Pérez-Torres, Coraly D. Velázquez-Díaz, Marcos J. Sánchez-Navarro, Carlos I. Huertas-Pérez, María M. Diehl, Mary L. Phillips, Suzanne N. Haber, and Gregory J. Quirk

ABSTRACT

BACKGROUND: A common symptom of obsessive-compulsive disorder is the persistent avoidance of cues incorrectly associated with negative outcomes. This maladaptation becomes increasingly evident as subjects fail to respond to extinction-based treatments such as exposure-with-response prevention therapy. While previous studies have highlighted the role of the insular-orbital cortex in fine-tuning avoidance-based decisions, little is known about the projections from this area that might modulate compulsive-like avoidance.

METHODS: Here, we used anatomical tract-tracing, single-unit recording, and optogenetics to characterize the projections from the insular-orbital cortex. To model exposure-with-response prevention and persistent avoidance in rats, we used the platform-mediated avoidance task followed by extinction-with-response prevention training.

RESULTS: Using tract-tracing and unit recording, we found that projections from the agranular insular/lateral orbital (AI/LO) cortex to the prefrontal cortex predominantly target the rostral portion of the prelimbic (rPL) cortex and excite rPL neurons. Photoinhibiting this projection induced persistent avoidance after extinction-with-response prevention training, an effect that was still present 1 week later. Consistent with this, photoexcitation of this projection prevented persistent avoidance in overtrained rats. This projection to rPL appears to be key for AI/LO's effects, considering that there was no effect of photoinhibiting AI/LO projections to the ventral striatum or basolateral amygdala.

CONCLUSIONS: Our findings suggest that projections from the AI/LO to the rPL decreases the likelihood of avoidance behavior following extinction. In humans, this connectivity may share some homology of projections from lateral prefrontal cortices (i.e., ventrolateral prefrontal cortex, orbitofrontal cortex, and insula) to other prefrontal areas and the anterior cingulate cortex, suggesting that reduced activity in these pathways may contribute to obsessive-compulsive disorder.

<https://doi.org/10.1016/j.biopsych.2022.02.008>

Obsessive-compulsive disorder (OCD) is commonly characterized by persistent recurrence of avoidance responses and excessive searching for safety, which provides temporary relief that perpetuates the obsessive-compulsive cycle (1–5). This maladaptation is particularly evident in patients with OCD who display deficits in decision making and fail to respond to extinction-based treatments such as exposure-with-response prevention (ERP) therapy (6–9). The ability of extinction learning to restore decision-making processes and suppress avoidance responses is critical for breaking the OCD cycle (10,11). Although previous studies have highlighted the role of the insular/orbital cortex in fine-tuning avoidance-based decisions in animals (12–16) and humans (including patients with OCD) (17–20), little is known about the influence of the insular/orbital cortex on prefrontal and limbic areas that modulate persistent avoidance.

Using platform-mediated avoidance (PMA) conditioning (21) followed by extinction-with-response prevention (Ext-RP)

training (12), we previously observed that overcoming persistent avoidance was correlated with increased activity of neurons in the agranular insular/lateral orbital (AI/LO) area and prelimbic (PL) prefrontal cortex (PFC) (22). Furthermore, avoidance responses in this task were correlated with inhibitory responses in rostral PL (rPL) but not in caudal PL (cPL) neurons (23), suggesting that AI/LO inputs might reduce persistent avoidance by activating rPL neurons. Consistent with this, pharmacological inactivation of the AI/LO induces persistent avoidance following Ext-RP (12). However, little is known about the role of specific projections of the AI/LO in persistent avoidance.

The PL cortex is necessary for the expression of PMA (21,23), and the AI/LO projects to the PL cortex (16,24–26). Studies across species highlight projections from the lateral prefrontal and insular cortices to the anterior cingulate cortex (ACC) (PL homolog) as part of the salience network (27–29), with the rostral ACC linked to cognitive control (i.e., choice

action) and the caudal ACC linked to action execution (i.e., motor reaction) (30). However, in rodents, the rostrocaudal boundaries of AI/LO projections within the PL and cingulate (Cg) cortices and the role of those projections in avoidance-based decisions is not known. Here, we used tract-tracing to characterize the rostrocaudal extent of AI/LO projections to the PL and Cg cortices. To determine the role of these projections in avoidance decisions, we used optogenetic manipulations of AI/LO outputs following the Ext-RP task. Understanding cortical circuits that modulate avoidance-based decisions might reveal innovative clinical targets for reducing compulsions in OCD.

METHODS AND MATERIALS

See the [Supplement](#) for the full methodological descriptions.

Subjects and Bar Press Training

Adult male Sprague Dawley rats (Envigo Laboratories) were restricted to 18 g/day of laboratory chow and trained to press a bar for sucrose pellets on a variable interval schedule-30 seconds. All procedures were approved by the Institutional Animal Care and Use Committee of the University of Puerto Rico School of Medicine and the Association for Assessment and Accreditation of Laboratory Animal Care.

Surgery

Rats were anesthetized with isoflurane gas and positioned in a stereotaxic frame. For anterograde tracing, rats were unilaterally infused in the AI/LO area (+3.24 mm anterior-posterior [AP]; ±3.15 mm medial-lateral [ML]; -6.00 mm dorsal-ventral [DV]) (31) with an anterograde virus (see below). For retrograde tracing, cholera toxin B (CTB) was unilaterally infused in the rPL (+4.40 mm AP; ±0.61 mm ML; -3.65 mm DV) or cPL (+2.76 mm AP; ±0.61 mm ML; -3.92 mm DV).

For optrode experiments, rats were bilaterally infused with a viral vector (archaerhodopsin [ArchT]) in the AI/LO area (+3.24 mm AP; ±3.15 mm ML; -6.00 mm DV). Rats were given 8 to 12 weeks for the viral expression before the optrode implantation and recordings in the rPL.

For optogenetic experiments, rats were bilaterally infused with viral vectors (halorhodopsin [eNpHR] or channelrhodopsin-2 [ChR2]) in the AI/LO area (+3.24 mm AP; ±3.15 mm ML; -6.00 mm DV). Optical fibers (length: 4 mm rPL, 8 mm ventral striatum [VS], 10 mm basolateral amygdala [BLA]; obtained from Thorlabs or Newdoon) were implanted (bilaterally) in the rPL, VS, or BLA for terminal illumination. The coordinates for each region are as follows: rPL, +4.2 mm AP, ±1.5 mm ML, -3.4 mm DV, at a 15° angle; VS, +1.2 mm AP, ±4.20/3.35 mm ML, -7.4 mm DV, at 20°/15° angles; and BLA, -2.76 mm AP, ±4.65 mm ML, -8.7 mm DV.

Tracer and Viruses

For anterograde tracing, an AAV5 (adeno-associated virus serotype 5) targeting glutamatergic neurons (32–34) and expressing EYFP (enhanced yellow fluorescent protein) (AAV5:CaMKIIa::EYFP; 3×10^{12} particles/mL) (UNC [University of North Carolina Vector Core]) was used for anterograde labeling in the rPL. While this serotype may display some retrograde properties (35), we did not see any sign of retrogradely

labeled cell bodies in our histological analyses (Figures 1 and 2; Figure S1). For retrograde tracing, CTB (555 nm; ThermoFisher) (36) was used for retrograde labeling in AI/LO cells.

For optogenetic and optrode experiments, AAV5 was used (UNC). Viral titers were approximately 4×10^{12} particles/mL for ChR2 (AAV5:CaMKIIa:hChR2(H134R)-EYFP), halorhodopsin (AAV5:CaMKIIa:eNpHR3.0-EYFP), and ArchT (optrodes) (AAV5:CaMKIIa:eArchT3.0-EYFP) and 3×10^{12} particles/mL for EYFP controls (AAV5:CaMKIIa::EYFP). For the optrode experiment, we used ArchT because we had some difficulty in obtaining neuronal responses using eNpHR. Thus, we decided to build on our previous experience using ArchT (23), which is robust in inhibiting neuronal terminals (37,38), to interrogate the role of AI/LO terminals in the rPL. For the behavioral assays, we continued using eNpHR because these experiments were initiated long before recording experiments.

Tracing and Viral Labeling

Viral anterograde labeling of AI/LO terminals in the PL-Cg axis was quantified as corrected total fluorescence (ImageJ; National Institutes of Health). The coordinates for the PL-Cg axis range from +4.68 to +2.28 AP, and those for the infusion site (AI/LO) are +3.24 mm AP; ±3.15 mm ML; and -6.00 mm DV (31).

CTB retrograde labeling in AI/LO area (+4.20 to +2.76 AP) from either rPL or cPL infusion was quantified as total number of labeled cells (ImageJ). Rats showing correct infusion sites within rPL (+4.68 to +3.24 AP) or cPL boundaries (+3.24 to +2.52 AP) were analyzed (31). Rats showing overlapping CTB spread between infusion sites were excluded.

Behavior

PMA conditioning was performed as previously described (21,22). Briefly, rats received nine tone-shock pairings each day for 8 or 20 days. An acrylic square platform was placed in the opposite corner of the sucrose-delivering bar to allow rats to avoid the shocks. For photoinhibition experiments, on day 9 (conditioning test), rats were given two tones (trials) without shocks where the first trial was under optogenetic manipulation and the time spent on the platform was measured. On day 10 or day 21, rats received Ext-RP training (4 days), in which 15 tones without shocks were delivered per day (Pavlovian extinction) while access to the platform was blocked with a plexiglass barrier, as previously described (12,22).

Following Ext-RP training, the barrier was then removed to assess extinction learning (post-Ext-RP). Similar to the conditioning test, in the first post-Ext-RP test (test 1; day 14 or 25), rats were given two tones (trials) without shocks where the first trial was under optogenetic manipulation and the time spent on the platform was measured. One week later (test 2), rats were given a single tone (no laser and no barrier) to test for long-term effects of optogenetic manipulation.

Laser Delivery

We used a diode pump solid state yellow laser (594 nm) for eNpHR, a diode pump solid state green laser (532 nm) for ArchT (recording experiment), and a diode pump solid state blue laser (473 nm) for ChR2 from OptoEngin LLC (23,39–41).

The laser and the tone were simultaneously activated at the first bar press after 3 minutes in the behavioral box and

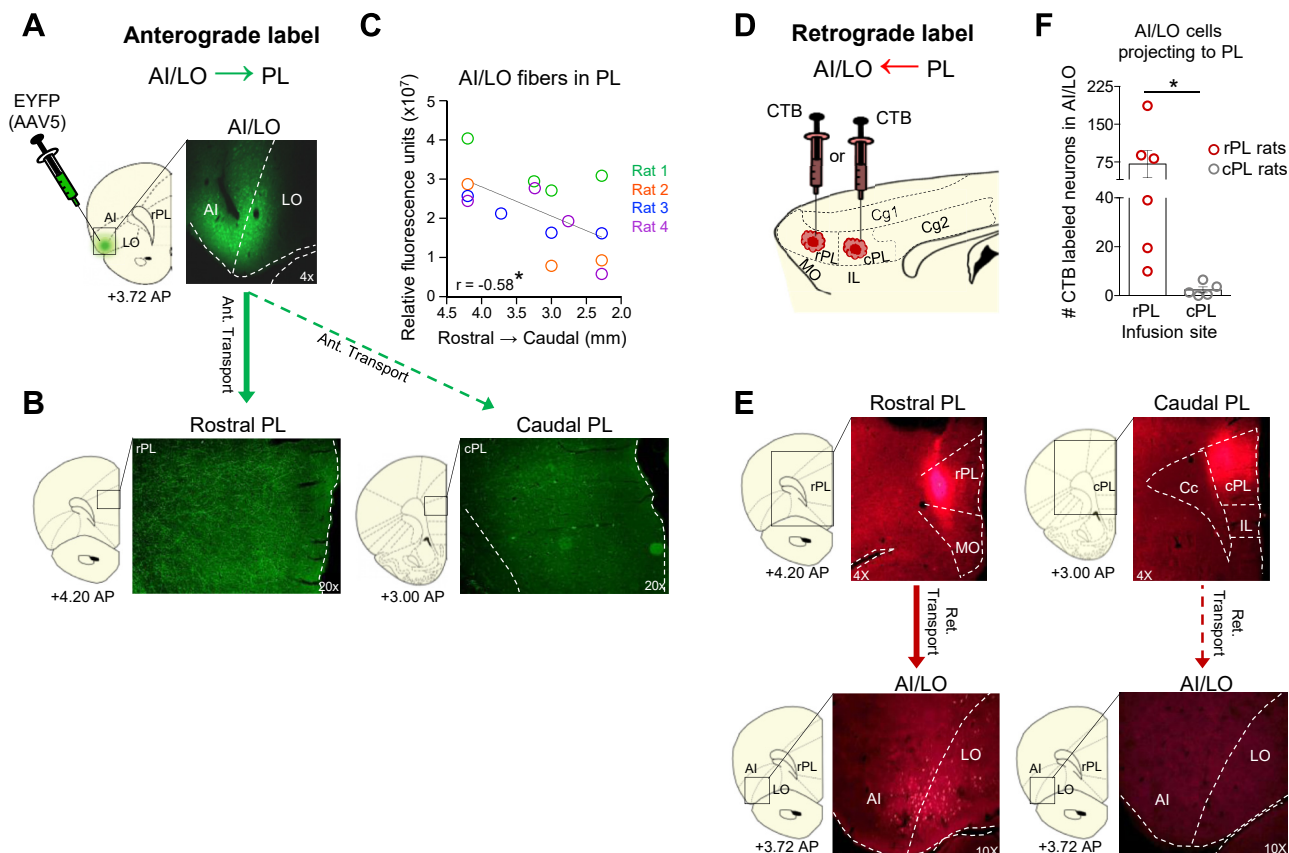


Figure 1. Anatomical tracing of AI/LO projections to the PL cortex. **(A)** Representative schematic and micrograph of the viral (AAV5:CaMKIIa:EYFP) infusion in the AI/LO area. **(B)** Anterograde viral labeling in the rPL and cPL cortex ($n = 4$). **(C)** Regression analysis showing a reduction in anterograde labeling from rostral to caudal along the PL-Cg axis ($n = 4$). **(D)** Schematic showing the infusion of retrograde tracer (CTB) into rPL or cPL. **(E)** Micrographs showing representative infusion sites in rPL or cPL (upper panel) and examples of retrogradely labeled neurons in the AI/LO (lower panel). **(F)** Infusion of tracer into the rPL resulted in more labeled neurons in the AI/LO compared with infusions into the cPL. rPL: $n = 6$; cPL: $n = 4$. All data are shown as mean \pm SEM. $*p < .05$. AI/LO, agranular insular/lateral orbital cortex; AP, anterior-posterior; Cc, corpus callosum; Cg, cingulate; cPL, caudal prelimbic; CTB, cholera toxin B; EYFP, enhanced yellow fluorescent protein; IL, infralimbic cortex; MO, medial orbitofrontal cortex; PL, prelimbic; rPL, rostral PL.

continued throughout the 30-second tone presentation. Laser light was passed through a shutter/coupler (Oz Optics), patchcord (ThorLabs), rotary joint (Doric Lenses), dual patchcord (ThorLabs), and bilateral optical fibers.

Optrode Recordings

Rats were anesthetized with urethane and mounted in a stereotaxic frame. A movable optrode consisting of an optical fiber surrounded by an array of 8 or 16 single-unit recording wires (Neuro Biological Lab) was aimed at the rPL (+4.2 to +3.3 mm AP; ± 0.6 mm ML; -3.5 to -4.5 mm DV). The optrode was moved in steps of 0.03 mm. After isolating a single unit (neurons in rPL; RASPUTIN; Plexon), a 532-nm laser was activated for 10 seconds within a 20-second period at least 10 times for AI/LO terminals expressing ArchT in the rPL. Single units were recorded and stored for spike sorting (Offline Sorter; Plexon) and spike-train analysis (Neuroexplorer; NEX Technologies). Excitatory (above baseline) and inhibitory (below baseline) responses were calculated by comparing the average firing rate of each neuron during the last 5 seconds of the laser OFF period (baseline) with the 10 seconds of laser ON

for rPL neurons (Mann-Whitney U test, 1-second bins). The average firing rate of each cell before (prelaser/baseline; OFF) and during the laser stimulation (ON) were also compared (Wilcoxon signed-rank test, 1-second bins). The use of the last 5 seconds as baseline (prelaser) was used to avoid rebound-related effects postlaser.

Open Field Task

At 24–48 hours after the last post-Ext-RP test (test 2), locomotor activity was assessed in EYFP-control and eNpHR or ChR2 groups (see the Supplement).

Histology

Rats were deeply anesthetized and perfused. Brains were removed and stored in cryoprotectant solution before sectioning (see the Supplement).

Data Collection and Analysis

Behavioral data were acquired using the Any-Maze software (Stoelting Co.). Statistical analyses included Student's two-

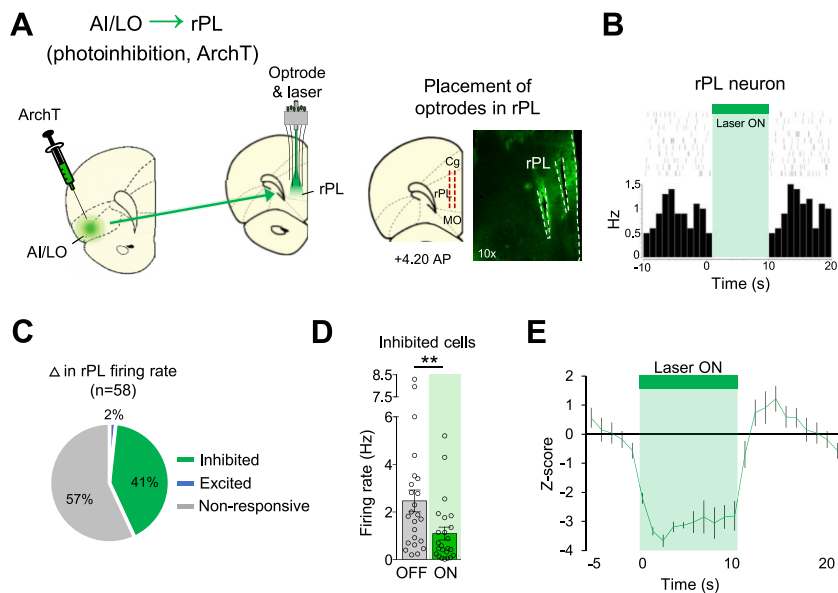


Figure 2. Photoinhibiting AI/LO projections to the rPL cortex reduces firing rate of rPL neurons. **(A)** Schematic and micrograph of viral (ArchT) infusion into AI/LO and representative optrode placement in the rPL cortex. **(B)** Raster and peristimulus time histogram of a representative rPL neuron showing a decrease in firing rate during laser illumination. **(C)** Photoinhibition of AI/LO–rPL projections (in anesthetized rats) significantly reduced the firing rate of 41% of single rPL neurons recorded. **(D)** Average firing rate before and during laser stimulation of neurons showing a significant reduction in rate. **(E)** Average firing rate of these neurons expressed as z scores. Rats: $n = 3$; cells: $n = 58$ neurons. All data are shown as mean \pm SEM. $**p < .01$. AI/LO, agranular insular/lateral orbital; AP, anterior-posterior; ArchT, archaerhodopsin; rPL, rostral PL.

tailed t test, Mann-Whitney U test, Wilcoxon signed-rank test, Pearson correlation, or two-way repeated-measures analyses of variance followed by post hoc Bonferroni analysis. Suppression of bar pressing was calculated as (pretone presses – tone presses)/(pretone presses + tone presses) \times 100. Data are presented as mean \pm SEM, and statistical significance was established as $*p < .05$ (Prism 6.0 software).

RESULTS

AI/LO Projections to the PL-Cg Axis Predominantly Target the rPL Cortex

To delineate the anatomical projections from the AI/LO to the rPL, cPL, and Cg, naïve rats were unilaterally infused with an anterograde tracer (AAV5:CaMKIIa:eYFP) in the AI/LO (Figure 1A). After 8 to 12 weeks, brains were collected to corroborate the infusion site in the AI/LO and analyze anterograde labeling of fibers along the PL-Cg axis (Figure 1A, B). Labeling of AI/LO fibers was significantly more abundant in the rPL than in either the cPL or Cg ($r = -0.58$, $p = .021$) (Figure 1C). To further corroborate these anterograde findings, a separate cohort of naïve rats was unilaterally infused with a retrograde tracer (CTB; 555) in either the rPL or cPL (Figure 1D). Three weeks later, brains were analyzed for retrogradely labeled neurons in the AI/LO (Figure 1E, upper and lower panels). Consistent with the anterograde findings, infusion of the retrograde tracer into the rPL resulted in significantly more labeled neurons in the AI/LO than infusions into the cPL ($t_9 = 2.33$, $p = .043$) (Figure 1F).

AI/LO Projections to the rPL Cortex Are Excitatory

Previous work has shown that long-range projections from the PL can be either excitatory or inhibitory (42). To determine the effect of AI/LO projections on rPL firing rate, ArchT was infused into the AI/LO area, and an optrode was implanted into the rPL

to record single neurons from anesthetized rats (Figure 2A; Figure S1A). Photoinhibition of AI/LO terminals in the rPL decreased the spontaneous firing rate of rPL neurons (24 of 58 neurons; Mann-Whitney and Wilcoxon signed-ranks test pairing pre- vs. laser activity of each unit using 1-second time bins, all p values $< .05$) (Figure 2B–E). There was only one neuron (1 of 58 neurons) showing significant increases in rate following photoinhibition, suggesting that AI/LO projections to the rPL are largely excitatory.

Photoinhibition of AI/LO Projections to the rPL Induces Persistent Avoidance

To determine the role of excitatory projections from the AI/LO to the rPL in modulating avoidance-based decisions, we optogenetically probed this pathway using either photoinhibition or photoexcitation (Figure 3A). Following viral infusions in the AI/LO and implantation of optic probes in the rPL (Figure S1B, C), rats were trained in PMA for 8 days. Photoinhibition was first applied shortly after conditioning to interrogate the role of AI/LO projections on avoidance expression (day 9; only for the photoinhibition experiments). This was followed by 4 days (days 10–13) of Ext-RP in which extinction trials were given while the platform was blocked with a plexiglass barrier to prevent avoidance behavior (12,22). Optogenetic manipulations were again applied for photoinhibition experiments (and for the first time in the photoexcitation experiment; see below) at the post-Ext-RP test to interrogate the role of AI/LO projections during the decision time point following barrier removal.

After 8 days of avoidance conditioning, photoinhibition of the AI/LO projections to the rPL had no effect on the expression of avoidance as compared with EYFP controls (day 9; $F_{1,26} = 0.26$, $p = .613$; tone 1/laser ON, $p > .99$ and tone 2/laser OFF, $p > .99$) (Figure 3C). Ext-RP was then performed for 4 days with the barrier inserted, where no significant differences

Insular/Orbital-Prelimbic Circuit and Avoidance

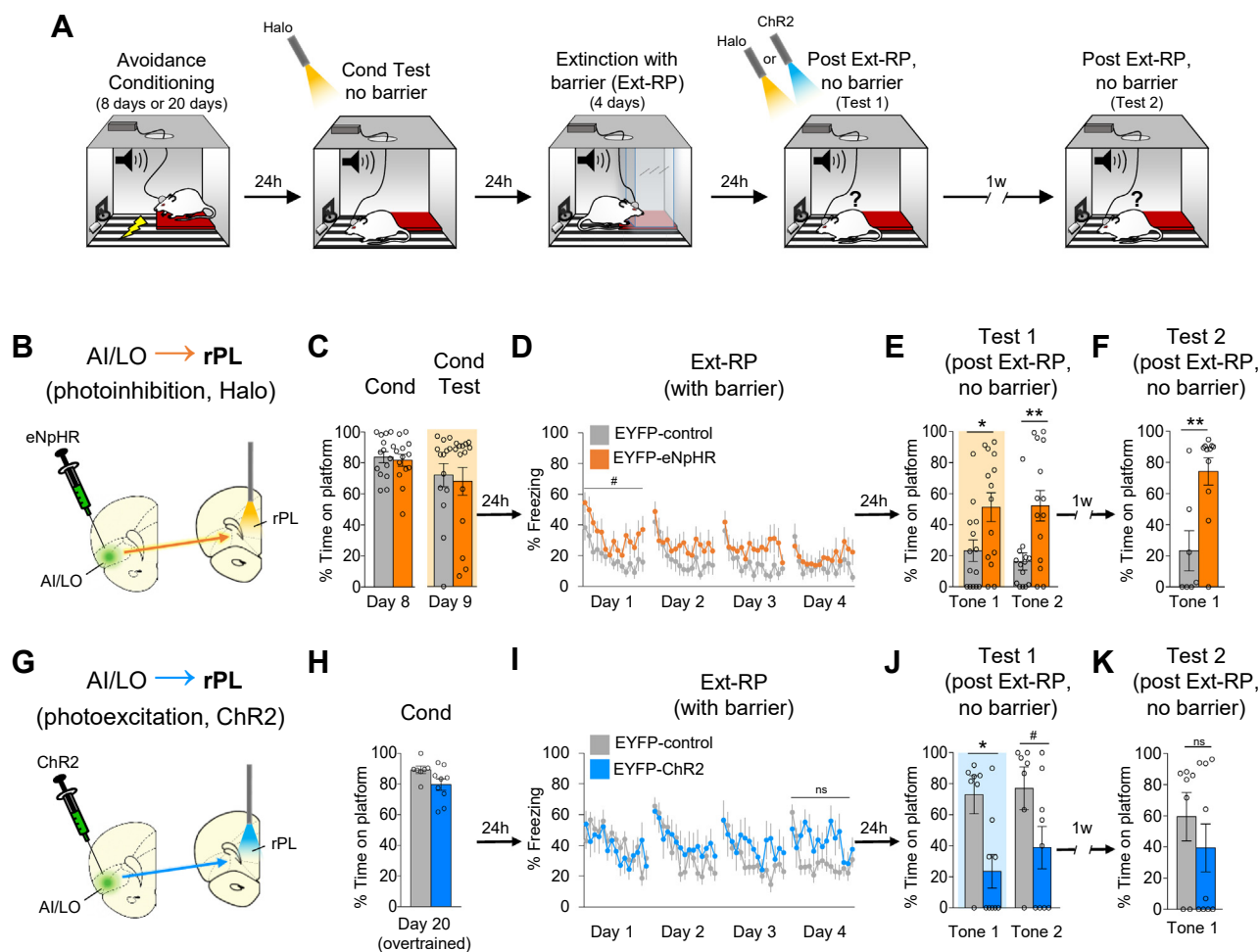


Figure 3. Optogenetic manipulations of the AI/LO–rPL cortex projection bidirectionally modulate persistent avoidance. **(A)** Schematic of the behavioral training: 1) platform-mediated avoidance conditioning (8 days for photoinhibition experiments or 20 days for the photoexcitation experiment), 2) post-conditioning test (only for photoinhibition experiments), 3) Ext-RP training with barrier present, and 4) post-Ext-RP tests with barrier removed and optogenetic manipulations (in either photoinhibition or -excitation). **(B)** Diagram illustrating the viral (Halo) infusion into the AI/LO and optic probe placement in the rPL. **(C)** After 8 days of avoidance conditioning, photoinhibition of AI/LO terminals had no effect on avoidance expression. **(D)** Extinction of freezing responses with barrier in place occurred over 4 days. **(E)** Photoinhibition of AI/LO–rPL projection induced persistent avoidance when rats were tested following Ext-RP with the barrier removed (test 1; laser ON). **(F)** This effect was still apparent 1 week later (test 2; laser OFF). **(G)** Schematic of viral infusion (ChR2) in AI/LO area and optic probe placement in the rPL. **(H, I)** Rats were given 20 days of overtraining in avoidance, followed by 4 days of extinction with the barrier in place. **(J)** Photoexcitation of AI/LO–rPL projection reduced persistent avoidance when rats were tested following Ext-RP with the barrier removed (test 1; laser ON). **(K)** This effect was no longer significant 1 week later (laser OFF). Photoinhibition experiments: EYFP-control: $n = 14$; EYFP-eNpHR: $n = 14$. Test 2: EYFP-control: $n = 7$; EYFP-eNpHR: $n = 11$. Photoexcitation experiment: EYFP-control: $n = 7$; EYFP-ChR2: $n = 9$. All data are shown as mean \pm SEM. $**p < .01$, $*p < .05$, $\#p \leq .09$, $^{ns}p > .1$ (nonsignificant). AI/LO, agranular insular/lateral orbital cortex; ChR2, channelrhodopsin-2; Cond, conditioning; eNpHR, halorhodopsin; Ext-RP, extinction-with-response prevention; EYFP, enhanced yellow fluorescent protein; Halo, halorhodopsin; rPL, rostral prelimbic.

were observed (Figure 3D; Figure S3B and Figure/Table S6, upper table). When the barrier was removed (test 1), photoinhibition of AI/LO projections to the rPL induced persistent avoidance, an effect that was maintained on the following trial with the laser OFF ($F_{1,26} = 13.79$, $p = .001$; tone 1/laser ON, $p = .036$, tone 2/laser OFF, $p = .005$) (Figure 3E; Figure S2 and Supplemental Video S1). Avoidance remained elevated in this group 7 days later in the absence of photoinhibition (test 2, laser OFF: $t_{16} = 3.32$, $p = .003$) (Figure 3F). Photoinhibition had no significant effect on freezing or bar pressing during the postconditioning test or the post-Ext-RP test (Figure S3B and Figure/Table S6, upper table). Similarly, photoinhibition of this

pathway had no effect on locomotion in an open field (all p values $> .05$) (Figure S5B and Figure/Table S6, upper table). Photoinhibition has been associated with postlaser rebound effects (37,38); however, there were no significant differences in our behavioral metrics between tone 1 and tone 2 (pretone 2) (Figure/Table S6, upper table).

Photoexcitation of AI/LO Projections to the rPL Cortex Prevents Persistent Avoidance

After inducing persistent avoidance with photoinhibition of AI/LO–rPL projection, we next asked if photoexcitation of this

projection would have the opposite effect (Figure 3G–K; Figure S1C). For this experiment, rats were overtrained on PMA (for 20 days instead of 8 days). We recently reported that overtraining increases the likelihood of persistent avoidance following Ext-RP, an effect that was accompanied by reduced activity (c-Fos) in AI/LO and PL areas (22). Because photo-inhibition did not show any significant effects at the post-conditioning time point, and to avoid affecting behavior at subsequent time points, we chose to initiate ChR2 excitation only during test 1 to reliably test the prediction from photo-inhibition that activity in this pathway reduces avoidance following Ext-RP.

In contrast to the effects of photoinhibition, photoexcitation of this circuit reduced avoidance at test, thereby preventing the effects of overtraining (test 1, $F_{1,14} = 7.423$, $p = .016$; tone 1/laser ON, $p = .021$, tone 2/laser OFF, $p = .086$) (Figure 3J; Figure S2 and Supplemental Video S2). Indeed, photoexcitation of AI/LO–rPL projections in rats trained for 20 days reduced the time spent on the platform to levels observed in EYFP-control rats that were trained for 8 days (23.6% vs. 23.2%). A significant reduction in persistent avoidance was no longer observed when rats were tested 1 week later in the absence of photostimulation (test 2/1 W: $t_{14} = 0.902$, $p = .381$) (Figure 3K).

Additional behavioral analyses revealed no significant effects of photoexcitation on freezing during the post-Ext-RP tests (all p values $> .05$) (Figure S3B and Figure/Table S6, lower table). However, photoexcitation induced a trend toward reduced suppression of bar pressing (Figure S3C and Figure/Table S6, lower table), which was accompanied by a significant reduction in avoidance during post-Ext-RP test 1 (laser ON) (Figure 3J), consistent with reduced fear. In the open field, photoexcitation induced a significant reduction in total distance traveled (locomotion) (Figure S5C and Figure/Table S6, lower table). However, during test 1, when photoexcitation decreased avoidance behavior, there was no significant difference in locomotion between groups (EYFP-control: $0.10 \text{ m} \pm 0.02$; EYFP-ChR2: $0.15 \text{ m} \pm 0.07$; $t_{14} = 0.58$, $p = .56$). No immediate poststimulation effects were observed during the intertone interval (pretone 2) (Figure/Table S6, lower table).

Photoinhibition of AI/LO Projections to the VS and BLA Had No Effect on Avoidance

The VS and BLA are critical for both the expression and extinction of avoidance behaviors (21,43–47), and these areas receive dense projections from the AI/LO (16,48–50). We therefore used the same optogenetic methods to interrogate AI/LO projections to these areas (Figure 4A). Following an infusion of halorhodopsin in the AI/LO area and implantation of optic probes in either the VS or BLA (Figure 4B, G; Figure S1D, E), rats received avoidance conditioning across 8 days followed by optogenetic manipulations during the post-conditioning and post-Ext-RP tests (Figure 4C–E, H–J). Photoinhibiting AI/LO projections to the VS had no effect on avoidance expression ($F_{1,25} = 0.935$, $p = .342$, tone 1/laser ON, $p > .99$, tone 2/laser OFF, $p = .413$) (Figure 4C) or during post-Ext-RP test 1 (test 1, $F_{1,25} = 0.11$, $p = .742$) or test 2 ($t_{25} = 0.827$, $p = .213$) (Figure 4E).

As for the AI/LO–BLA projection, there was no effect of photoinhibition on avoidance expression ($F_{1,21} = 0.552$, $p = .465$, tone 1/laser ON, $p = .720$, tone 2/laser OFF, $p > .999$) (Figure 4G) or during post-Ext-RP test 1 (test 1, $F_{1,21} = 3.087$, $p = .093$) or test 2/1 W ($t_{21} = 1.466$, $p = .157$) (Figure 4J). The lack of optogenetic effects on these two AI/LO projections highlights the rPL as a pivotal node in the AI/LO regulation of avoidance-based decisions.

There was also no effect of photoinhibition of AI/LO projections to the VS or BLA on freezing (Figure S4). However, a significant increase in suppression for bar pressing was observed during tone 2 (laser OFF) after inhibition of the AI/LO–BLA projection (Figure S4C and Figure/Table S7, lower table). Because this effect was not apparent in tone 1 (laser ON), this effect may be attributable to rebound excitation. Consistent with this, an increase in avoidance behavior was observed during the intertone interval (pretone 2) (Figure/Table S7, lower table). No postlaser effects were observed with the AI/LO–VS projection. Furthermore, there was no effect of photoinhibition of either projection on locomotion on the open field test (all p values $> .05$) (Figure S5D, E and Figure/Table S7).

DISCUSSION

Using a rodent model of ERP for avoidance-like OCD behaviors, we demonstrated that persistent avoidance is prevented by activity within AI/LO inputs to the PL cortex. We observed that the AI/LO predominantly targets the rPL via an excitatory pathway. Optogenetic manipulations revealed that activation of AI/LO inputs to the rPL is necessary for reducing persistent avoidance following Ext-RP. Combined, these findings demonstrate a novel circuit gating maladaptive avoidance behavior at a key decision point following extinction training. We further suggest that activity within this projection reduces the tendency to avoid when an animal is challenged by environmental cues.

Prior anatomical studies of the rodent frontal cortex have mostly focused on the medial FPC (51,52) with less emphasis on the insular/orbital circuits. Here, we found that AI/LO projections displayed a rostrocaudal gradient within the PL–Cg axis, with rPL being the predominant target. A similar finding in rats can be seen from the data of Hoover and Vertes (24), where infusion of retrograde tracers into the rPL labeled neurons in the AI/LO and insular areas. In contrast, limited retrograde labeling was observed in the AI/LO after infusions in the Cg or in the infralimbic cortex (24). Whereas the AI/LO sends excitatory projections to prefrontal areas, it also receives inputs in a cell-specific manner from these same cortical regions (25,53). Thus, reciprocal connections between the prefrontal areas, which integrate salience signals to guide behavior (54), may be responsible for fine-tuning approach and avoidance decisions.

The AI/LO has been previously associated with decision making and OCD-like behaviors. Inactivating the AI/LO induced persistent pressing of a lever previously associated with punishment (14) as well as persistent pressing of a rewarding lever following devaluation (55). Similarly, in the PMA task, pharmacological inactivation of the AI/LO induced persistent avoidance (12), and rats showing low levels of avoidance after Ext-RP showed increased activity in both the

Insular/Orbital-Prelimbic Circuit and Avoidance

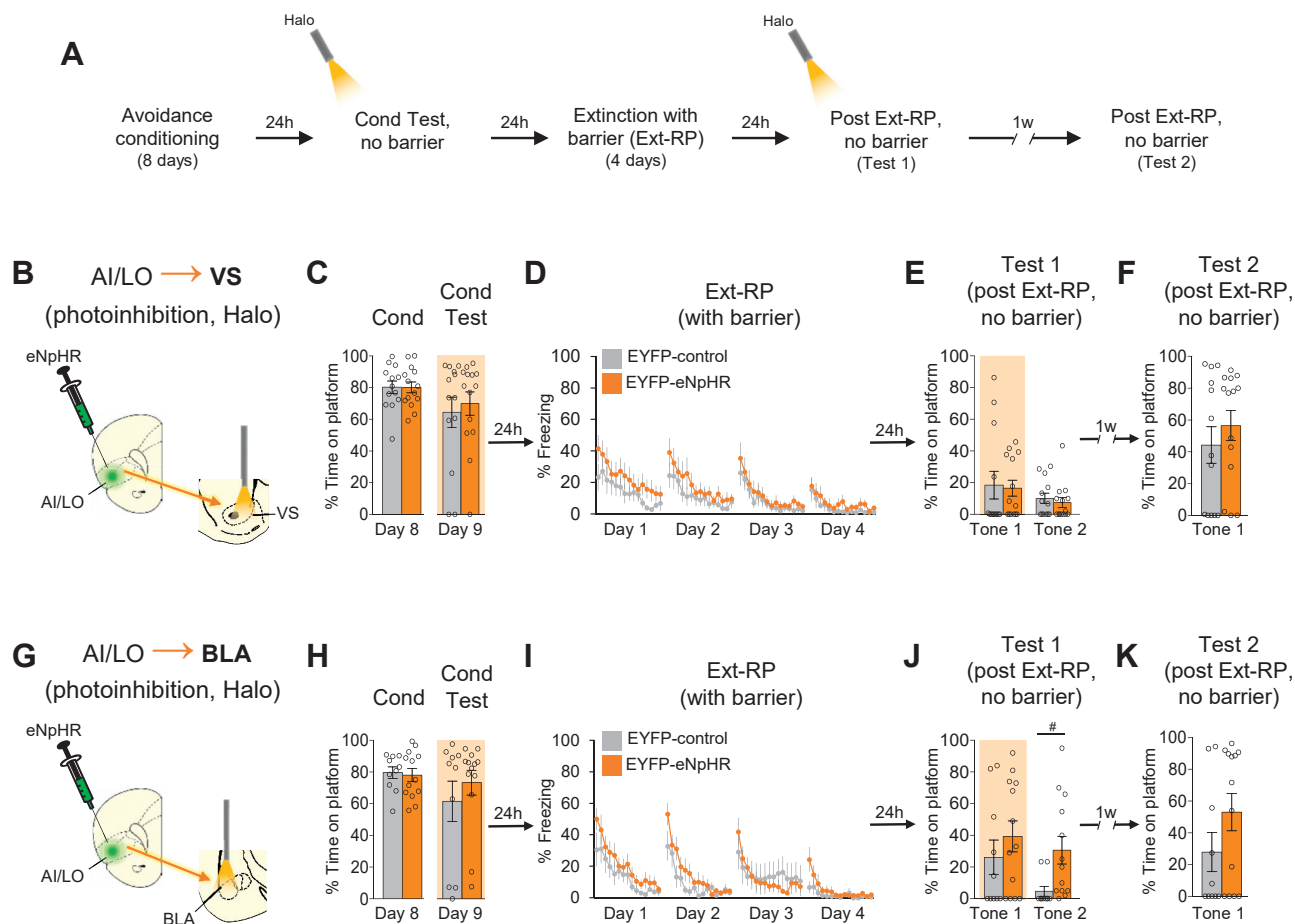


Figure 4. Photoinhibiting AI/LO projections to the VS or BLA had no effect on avoidance. **(A)** Schematic of the behavioral training: 1) platform-mediated avoidance conditioning (8 days), 2) postconditioning test (with optogenetic manipulations; photoinhibition), 3) Ext-RP training with barrier present, and 4) post-Ext-RP tests with barrier removed and optogenetic manipulations (photoinhibition). **(B)** Diagram illustrating the viral (Halo) infusion into the AI/LO and optic probe placement in the VS. **(C–F)** After 8 days of avoidance conditioning, photoinhibition of AI/LO terminals in the VS had no effect on avoidance expression, Ext-RP, or extinction tests 1 or 2. **(G)** Diagram illustrating the viral (Halo) infusion into the AI/LO and optic probe placement in the BLA. **(H–K)** After 8 days of avoidance conditioning, photoinhibition of AI/LO terminals in the BLA had no significant effect on avoidance expression, Ext-RP, or extinction tests 1 or 2. AI/LO–VS: EYFP-control: $n = 13$; eNpHR: $n = 14$. AI/LO–BLA: EYFP-control: $n = 10$; EYFP-eNpHR: $n = 13$. All data are shown as mean \pm SEM. $^{\#}p \leq .09$. AI/LO, agranular insular/lateral orbital cortex; BLA, basolateral amygdala; Cond, conditioning; eNpHR, halorhodopsin; Ext-RP; extinction-with-response prevention; EYFP, enhanced yellow fluorescent protein; Halo, halorhodopsin; VS, ventral striatum.

AI/LO and PL cortex (22). Photoactivation of AI/LO projections to the striatum has been shown to suppress OCD-like behavior in mice (i.e., excessive grooming) (40). Thus, there is a growing body of evidence suggesting that AI/LO projections reduce behaviors (appetitive or aversive) that are no longer appropriate. It should be noted that while most of the significant effects of the AI/LO projections were related to avoidance, some changes in the approach component (suppression, bar pressing) were also observed. This provides valuable information on how the AI/LO and its targets may impact the approach/avoidance balance under conflict scenarios (56).

Active avoidance depends on excitatory inputs to the VS from the BLA (43,57). In the PMA task, tone-signaled avoidance behavior is associated with inhibitory responses in rPL neurons (23), suggesting that a reduction in the firing rate of rPL neurons may disinhibit downstream neurons in the VS to

drive avoidance. Indeed, photoexcitation of rPL projections to the VS decreased avoidance in the PMA task (57). Consistent with feed-forward inhibition of avoidance by the rPL, we observed that optogenetic excitation of the AI/LO–rPL pathway reduced avoidance following removal of the barrier. These and the present findings suggest a model in which AI/LO modulation of the VS (via rPL) gates inputs coming from BLA, thereby preventing persistent avoidance at key decision points (Figure 5) [see also (21,23,45,57)]. While we observed some long-term plasticity effects of AI/LO–rPL photoinhibition (tone 2 and test 2), it remains to be determined whether these effects required co-presentation of the laser with tone 1 or whether post-tone laser exposure would have yielded similar effects.

In humans, hyperactivity in striatal, orbital, insular, and prefrontal areas (i.e., ACC) has been associated with OCD

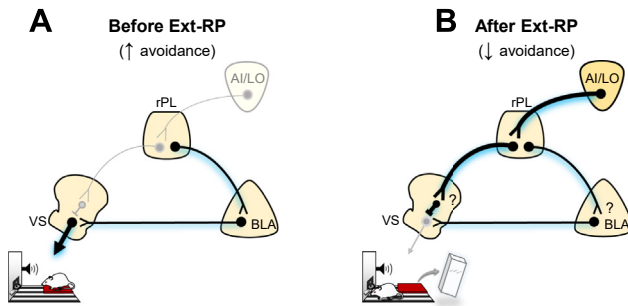


Figure 5. Proposed model of circuit gating persistent avoidance. **(A)** A hypothetical model illustrating a three-component circuit for the expression of avoidance. Before extinction (Ext-RP), the rPL cortex sends excitatory inputs to the BLA, and the BLA sends excitatory inputs to the VS to drive avoidance expression. rPL projections to VS inhibitory interneurons are dampened. **(B)** After Ext-RP, AI/LO neurons are recruited to activate rPL neurons that project to the VS, reducing the effect of BLA inputs to VS and inhibiting avoidance expression. AI/LO, agranular insular/lateral orbital cortex; BLA, basolateral amygdala; Ext-RP, extinction-with-response prevention; rPL, rostral prelimbic; VS, ventral striatum.

(58–62). However, recent studies link hypoactivity of the most lateral areas of the PFC (i.e., ventrolateral PFC [vIPFC] and dorsolateral PFC), including the inferior frontal gyrus and insula, to the OCD spectrum (20,63,64). A recent report showed that persistent avoidance in OCD patients is associated with reduced activity in insular, inferior frontal gyrus (including vIPFC), and orbital cortices, as well as deficits in the devaluation of negative stimuli (20). Moreover, resting-state functional magnetic resonance imaging analyses show reduced activity in the vIPFC and reduced connectivity with striatal areas in OCD (65,66). Subjects with OCD who were predisposed to form habits displayed decreased inferior frontal gyrus activity as well as negative coupling with the striatum (67).

There is some controversy concerning the homologies of areas comprising the PFC across species (i.e., humans, nonhuman primates [NHPs] and rodents) (68). However, there are anatomical and functional similarities that facilitate the interpretation of our results. For example, the PL cortex in rodents is broadly related to the ACC in humans and NHPs (30,68–72). Still, it is more difficult to assign homology of the rodent AI/LO to lateral prefrontal (i.e., vIPFC, orbitofrontal cortex) and insular regions in humans/NHPs (68–70). While AI/LO shares cytoarchitectonic similarity with the human/NHP anterior insular cortex (73), no such similarity exists with the lateral PFC. However, similarities in connectivity profiles have been used to address possible homologies across species. For example, similar profiles between the AI/LO and lateral prefrontal/insular cortices with thalamic and limbic structures are classically used to relate these regions to human areas (16,30,68–71). There is strong connectivity between the vIPFC/insula and ACC regions in both humans and NHPs (74,75). The strength of this connection is also seen in rodents between the AI/LO and PL cortex (16,25,53,54). Together, our findings with the AI/LO–rPL circuit in rodents suggest that the human insular-cingulate circuit might represent a new treatment target for OCD.

A common behavioral treatment for OCD is ERP (76,77), which could be improved with adjunct medications and/or brain stimulation (78). Our findings suggest that activating the vIPFC and insular areas might improve clinical outcomes in ERP. However, because we observed that the reduction in persistent avoidance after photoexcitation of the AI/LO–rPL projection waned over time, multiple stimulation sessions might be necessary to obtain the desired clinical outcome (i.e., less avoidance). Repetitive transcranial magnetic stimulation over the dorsolateral PFC/orbitofrontal cortex has been shown to ameliorate OCD symptoms (79,80). Similar results with the dorsolateral PFC have been observed with transcranial direct-current stimulation (81–83); however, such techniques have not yet targeted the insula or vIPFC for OCD. Our findings suggest that potentiating excitatory transmission from insula/vIPFC areas to rostral cingulate areas associated with cognitive control (30) might reduce OCD compulsions.

ACKNOWLEDGMENTS AND DISCLOSURES

This work was supported by the National Institutes of Health (Grant No. R37-MH058883 [to GJQ]; Conte Center Grant No. P50-MH106435 [to GJQ, MLP, and SNH]; Grant Nos. R37-MH100041, R01-MH060952, R01-MH059929, R01-MH115466, and R01-MH122990 [to MLP]; NeuroID Grant No. R25-NS080687 [to MJS-N]), the Pittsburgh Foundation (to MLP), and the University of Puerto Rico President's Office (to GJQ).

Part of the reported data was previously presented at the 2020 American College of Neuropsychopharmacology annual meeting.

We thank Tatiana Pelegrina, Carlos J. Rodríguez-Maldonado, and Zarkalys N. Quintero-Martínez for experimental and technical assistance. This work represents the final research paper from the Quirk Laboratory in Puerto Rico. Much appreciation to the outstanding trainees, colleagues, and staff here for their work over the past 25 years.

The authors report no biomedical financial interests or potential conflicts of interest.

ARTICLE INFORMATION

From the Departments of Psychiatry and Anatomy & Neurobiology (FJM-R, JP-T, CDV-D, MJS-N, CIH-P, MMD, GJQ), School of Medicine, Medical Sciences Campus, University of Puerto Rico, San Juan, Puerto Rico; Department of Psychiatry (MLP), University of Pittsburgh School of Medicine, Pittsburgh, Pennsylvania; Department of Pharmacology and Physiology (SNH), University of Rochester School of Medicine, Rochester, New York; and the McLean Hospital (SNH), Harvard Medical School, Belmont, Massachusetts.

FJM-R is currently affiliated with the Department of Neuroscience, Icahn School of Medicine at Mount Sinai, New York, New York. MMD is currently affiliated with the Department of Psychological Sciences, Kansas State University, Manhattan, Kansas.

Address correspondence to Freddyson J. Martínez-Rivera, Ph.D., at freddyson.martinez-rivera@mssm.edu.

Received Aug 23, 2021; revised Jan 24, 2022; accepted Feb 11, 2022.

Supplementary material cited in this article is available online at <https://doi.org/10.1016/j.biopsych.2022.02.008>.

REFERENCES

- Gillan CM, Morein-Zamir S, Urcelay GP, Sule A, Voon V, Apergis-Schoute AM, *et al.* (2014): Enhanced avoidance habits in obsessive-compulsive disorder. *Biol Psychiatry* 75:631–638.
- Veale D (2004): Psychopathology of obsessive-compulsive disorder. *Psychiatry* 3:65–68.
- Apergis-Schoute AM, Gillan CM, Fineberg NA, Fernandez-Egea E, Sahakian BJ, Robbins TW (2017): Neural basis of impaired safety signaling in obsessive compulsive disorder. *Proc Natl Acad Sci U S A* 114:3216–3221.

Insular/Orbital-Prelimbic Circuit and Avoidance

4. From the American Association of Neurological Surgeons (AANS), American Society of Neuroradiology (ASNR), Cardiovascular and Interventional Radiology Society of Europe (CIRSE), Canadian Interventional Radiology Association (CIRA), Congress of Neurological Surgeons (CNS), European Society of Minimally Invasive Neurological Therapy (ESMINT), European Society of Neuroradiology (ESNR), European Stroke Organization (ESO), Society for Cardiovascular Angiography and Interventions (SCAI), Society of Interventional Radiology (SIR), Society of NeuroInterventional Surgery (SNIS), and World Stroke Organization (WSO), Sacks D, Baxter B, Campbell BCV, Carpenter JS, Cognard C, *et al.* (2018): Multisociety consensus quality improvement revised consensus statement for endovascular therapy of acute ischemic stroke. *Int J Stroke* 13:612–632.
5. Hauser TU, Eldar E, Dolan RJ (2016): Neural mechanisms of harm-avoidance learning: A model for obsessive-compulsive disorder? *JAMA Psychiatry* 73:1196–1197.
6. Milad MR, Furtak SC, Greenberg JL, Keshaviah A, Im JJ, Falkenstein MJ, *et al.* (2013): Deficits in conditioned fear extinction in obsessive-compulsive disorder and neurobiological changes in the fear circuit. *JAMA Psychiatry* 70:608–618; quiz 554.
7. Hamatani S, Tsuchiyagaito A, Nihei M, Hayashi Y, Yoshida T, Takahashi J, *et al.* (2020): Predictors of response to exposure and response prevention-based cognitive behavioral therapy for obsessive-compulsive disorder. *BMC Psychiatry* 20:433.
8. Kyrios M, Hordern C, Fassnacht DB (2015): Predictors of response to cognitive behaviour therapy for obsessive-compulsive disorder. *Int J Clin Health Psychol* 15:181–190.
9. Nestadt G, Kamath V, Maher BS, Krasnow J, Nestadt P, Wang Y, *et al.* (2016): Doubt and the decision-making process in obsessive-compulsive disorder. *Med Hypotheses* 96:1–4.
10. Arch JJ, Abramowitz JS (2015): Exposure therapy for obsessive-compulsive disorder: An optimizing inhibitory learning approach. *J Obsessive Compulsive Relat Disord* 6:174–182.
11. Treanor M, Barry TJ (2017): Treatment of avoidance behavior as an adjunct to exposure therapy: Insights from modern learning theory. *Behav Res Ther* 96:30–36.
12. Rodríguez-Romaguera J, Greenberg BD, Rasmussen SA, Quirk GJ (2016): An avoidance-based rodent model of exposure with response prevention therapy for obsessive-compulsive disorder. *Biol Psychiatry* 80:534–540.
13. Daniel ML, Cocker PJ, Lacoste J, Mar AC, Houeto JL, Belin-Rauscent A, Belin D (2017): The anterior insula bidirectionally modulates cost-benefit decision-making on a rodent gambling task. *Eur J Neurosci* 46:2620–2628.
14. Jean-Richard-Dit-Bressel P, McNally GP (2016): Lateral, not medial, prefrontal cortex contributes to punishment and aversive instrumental learning. *Learn Mem* 23:607–617.
15. Saga Y, Ruff CC, Tremblay L (2019): Disturbance of approach-avoidance behaviors in non-human primates by stimulation of the limbic territories of basal ganglia and anterior insula. *Eur J Neurosci* 49:687–700.
16. Gogolla N (2017): The insular cortex. *Curr Biol* 27:R580–R586.
17. Aupperle RL, Paulus MP (2010): Neural systems underlying approach and avoidance in anxiety disorders. *Dialogues Clin Neurosci* 12:517–531.
18. Palminteri S, Justo D, Jauffret C, Pavlicek B, Dauta A, Delmaire C, *et al.* (2012): Critical roles for anterior insula and dorsal striatum in punishment-based avoidance learning. *Neuron* 76:998–1009.
19. Norbury A, Robbins TW, Seymour B (2018): Value generalization in human avoidance learning. *Elife* 7:e34779.
20. Chase HW, Graur S, Versace A, Greenberg T, Bonar L, Hudak R, *et al.* (2020): Neural mechanisms of persistent avoidance in OCD: A novel avoidance devaluation study. *Neuroimage Clin* 28:102404.
21. Bravo-Rivera C, Roman-Ortiz C, Brignoni-Perez E, Sotres-Bayon F, Quirk GJ (2014): Neural structures mediating expression and extinction of platform-mediated avoidance. *J Neurosci* 34:9736–9742.
22. Martínez-Rivera FJ, Sánchez-Navarro MJ, Huertas-Pérez CI, Greenberg BD, Rasmussen SA, Quirk GJ (2020): Prolonged avoidance training exacerbates OCD-like behaviors in a rodent model. *Transl Psychiatry* 10:212.
23. Diehl MM, Bravo-Rivera C, Rodríguez-Romaguera J, Pagan-Rivera PA, Burgos-Robles A, Roman-Ortiz C, Quirk GJ (2018): Active avoidance requires inhibitory signaling in the rodent prelimbic prefrontal cortex. *Elife* 7:e34657.
24. Hoover WB, Vertes RP (2007): Anatomical analysis of afferent projections to the medial prefrontal cortex in the rat. *Brain Struct Funct* 212:149–179.
25. Gehrlach DA, Weiland C, Gaitanos TN, Cho E, Klein AS, Hennrich AA, *et al.* (2020): A whole-brain connectivity map of mouse insular cortex. *Elife* 9:e55585.
26. Medford N, Critchley HD (2010): Conjoint activity of anterior insular and anterior cingulate cortex: Awareness and response. *Brain Struct Funct* 214:535–549.
27. Seeley WW (2019): The salience network: A neural system for perceiving and responding to homeostatic demands. *J Neurosci* 39:9878–9882.
28. Menon V, Uddin LQ (2010): Saliency, switching, attention and control: A network model of insula function. *Brain Struct Funct* 214:655–667.
29. Tsai PJ, Keeley RJ, Carmack SA, Vendruscolo JCM, Lu H, Gu H, *et al.* (2020): Converging structural and functional evidence for a rat salience network. *Biol Psychiatry* 88:867–878.
30. Tang W, Jbabdi S, Zhu Z, Cottaar M, Grisot G, Lehman JF, *et al.* (2019): A connective hub in the rostral anterior cingulate cortex links areas of emotion and cognitive control. *Elife* 8:e43761.
31. Paxinos G, Watson C (2007): *The Rat Brain in Stereotaxic Coordinates*, 6th ed. New York: Academic Press.
32. Liu XB, Jones EG (1996): Localization of alpha type II calcium calmodulin-dependent protein kinase at glutamatergic but not gamma-aminobutyric acid (GABAergic) synapses in thalamus and cerebral cortex. *Proc Natl Acad Sci U S A* 93:7332–7336.
33. Warthen DM, Lambeth PS, Ottolini M, Shi Y, Barker BS, Gaykema RP, *et al.* (2016): Activation of pyramidal neurons in mouse medial prefrontal cortex enhances food-seeking behavior while reducing impulsivity in the absence of an effect on food intake. *Front Behav Neurosci* 10:63.
34. Van den Oever MC, Rotaru DC, Heinsbroek JA, Gouwenberg Y, Deisseroth K, Stuber GD, *et al.* (2013): Ventromedial prefrontal cortex pyramidal cells have a temporal dynamic role in recall and extinction of cocaine-associated memory. *J Neurosci* 33:18225–18233.
35. Aschauer DF, Kreuz S, Rumpel S (2013): Analysis of transduction efficiency, tropism and axonal transport of AAV serotypes 1, 2, 5, 6, 8 and 9 in the mouse brain. *PLoS One* 8:e76310.
36. Conte WL, Kamishina H, Reep RL (2009): Multiple neuroanatomical tract-tracing using fluorescent Alexa Fluor conjugates of cholera toxin subunit B in rats. *Nat Protoc* 4:1157–1166.
37. Mahn M, Prigge M, Ron S, Levy R, Yizhar O (2016): Biophysical constraints of optogenetic inhibition at presynaptic terminals. *Nat Neurosci* 19:554–556.
38. Wiegert JS, Oertner TG (2016): How (not) to silence long-range projections with light. *Nat Neurosci* 19:527–528.
39. Do-Monte FH, Manzano-Nieves G, Quiñones-Laracueno K, Ramos-Medina L, Quirk GJ (2015): Revisiting the role of infralimbic cortex in fear extinction with optogenetics. *J Neurosci* 35:3607–3615.
40. Burguière E, Monteiro P, Feng G, Graybiel AM (2013): Optogenetic stimulation of lateral orbitofronto-striatal pathway suppresses compulsive behaviors. *Science* 340:1243–1246.
41. Ahmari SE, Spellman T, Douglass NL, Kheirbek MA, Simpson HB, Deisseroth K, *et al.* (2013): Repeated cortico-striatal stimulation generates persistent OCD-like behavior. *Science* 340:1234–1239.
42. Lee AT, Vogt D, Rubenstein JL, Sohal VS (2014): A class of GABAergic neurons in the prefrontal cortex sends long-range projections to the nucleus accumbens and elicits acute avoidance behavior. *J Neurosci* 34:11519–11525.
43. Ramirez F, Moscarello JM, LeDoux JE, Sears RM (2015): Active avoidance requires a serial basal amygdala to nucleus accumbens shell circuit. *J Neurosci* 35:3470–3477.

44. Martinez RCR, Gupta N, Lázaro-Muñoz G, Sears RM, Kim S, Moscarello JM, *et al.* (2013): Active vs. reactive threat responding is associated with differential c-Fos expression in specific regions of amygdala and prefrontal cortex. *Learn Mem* 20:446–452.
45. LeDoux JE, Moscarello J, Sears R, Campese V (2017): The birth, death and resurrection of avoidance: A reconceptualization of a troubled paradigm. *Mol Psychiatry* 22:24–36.
46. Cain CK (2019): Avoidance problems reconsidered. *Curr Opin Behav Sci* 26:9–17.
47. Moscarello JM, Maren S (2018): Flexibility in the face of fear: Hippocampal-prefrontal regulation of fear and avoidance. *Curr Opin Behav Sci* 19:44–49.
48. Groman SM, Keistler C, Keip AJ, Hammarlund E, DiLeone RJ, Pittenger C, *et al.* (2019): Orbitofrontal circuits control multiple reinforcement-learning processes. *Neuron* 103:734–746.e3.
49. Chikama M, McFarland NR, Amaral DG, Haber SN (1997): Insular cortical projections to functional regions of the striatum correlate with cortical cytoarchitectonic organization in the primate. *J Neurosci* 17:9686–9705.
50. Barreiros IV, Panayi MC, Walton ME (2021): Organization of afferents along the anterior-posterior and medial-lateral axes of the rat orbitofrontal cortex. *Neuroscience* 460:53–68.
51. Vertes RP (2004): Differential projections of the infralimbic and pre- limbic cortex in the rat. *Synapse* 51:32–58.
52. Gabbott PLA, Warner TA, Jays PRL, Salway P, Busby SJ (2005): Prefrontal cortex in the rat: Projections to subcortical autonomic, motor, and limbic centers. *J Comp Neurol* 492:145–177.
53. Murphy MJM, Deutch AY (2018): Organization of afferents to the orbitofrontal cortex in the rat. *J Comp Neurol* 526:1498–1526.
54. Uddin LQ (2015): Saliency processing and insular cortical function and dysfunction. *Nat Rev Neurosci* 16:55–61.
55. Parkes SL, Ravassard PM, Cerpa JC, Wolff M, Ferreira G, Coutureau E (2018): Insular and ventrolateral orbitofrontal cortices differentially contribute to goal-directed behavior in rodents. *Cereb Cortex* 28:2313–2325.
56. Bravo-Rivera H, Rubio Arzola P, Caban-Murillo A, Vélez-Avilés AN, Ayala-Rosario SN, Quirk GJ (2021): Characterizing different strategies for resolving approach-avoidance conflict. *Front Neurosci* 15:608922.
57. Diehl MM, Iravedra-García JM, Morán-Sierra J, Rojas-Bowe G, Gonzalez-Diaz FN, Valentín-Valentín VP, Quirk GJ (2020): Divergent projections of the pre- limbic cortex bidirectionally regulate active avoidance. *Elife* 9:e59281.
58. Haber SN (2017): Neurocircuitry underlying OCD: Neural networks underlying reward and action selection. In: Pittenger C, editor. *Obsessive-Compulsive Disorder: Phenomenology, Pathophysiology, and Treatment*. Oxford: Oxford University Press, 201–212.
59. Nakao T, Okada K, Kanba S (2014): Neurobiological model of obsessive-compulsive disorder: Evidence from recent neuropsychological and neuroimaging findings. *Psychiatry Clin Neurosci* 68:587–605.
60. Fitzgerald KD, Welsh RC, Gehring WJ, Abelson JL, Himle JA, Liberzon I, Taylor SF (2005): Error-related hyperactivity of the anterior cingulate cortex in obsessive-compulsive disorder. *Biol Psychiatry* 57:287–294.
61. Medvedeva NS, Masharipov RS, Korotkov AD, Kireev MV, Medvedev SV (2020): Dynamics of activity in the anterior cingulate cortex on development of obsessive-compulsive disorder: A combined PET and fMRI study. *Neurosci Behav Physiol* 50:298–305.
62. Luijckes J, Figeo M, Tobler PN, van den Brink W, de Kwaasteniet B, van Wingen G, Denys D (2016): Doubt in the insula: Risk processing in obsessive-compulsive disorder. *Front Hum Neurosci* 10:283.
63. Chen Y, Meng X, Hu Q, Cui H, Ding Y, Kang L, *et al.* (2016): Altered resting-state functional organization within the central executive network in obsessive-compulsive disorder. *Psychiatry Clin Neurosci* 70:448–456.
64. Robbins TW, Vaghi MM, Banca P (2019): Obsessive-compulsive disorder: Puzzles and prospects. *Neuron* 102:27–47.
65. Vaghi MM, Vértes PE, Kitzbichler MG, Apergis-Schoute AM, van der Flier FE, Fineberg NA, *et al.* (2017): Specific frontostriatal circuits for impaired cognitive flexibility and goal-directed planning in obsessive-compulsive disorder: Evidence from resting-state functional connectivity. *Biol Psychiatry* 81:708–717.
66. Anticevic A, Hu S, Zhang S, Savic A, Billingslea E, Wasylink S, *et al.* (2014): Global resting-state functional magnetic resonance imaging analysis identifies frontal cortex, striatal, and cerebellar dysconnectivity in obsessive-compulsive disorder. *Biol Psychiatry* 75:595–605.
67. Gillan CM, Apergis-Schoute AM, Morein-Zamir S, Urcelay GP, Sule A, Fineberg NA, *et al.* (2015): Functional neuroimaging of avoidance habits in obsessive-compulsive disorder. *Am J Psychiatry* 172:284–293.
68. Carlén M (2017): What constitutes the prefrontal cortex? *Science* 358:478–482.
69. Preuss TM, Wise SP (2022): Evolution of prefrontal cortex. *Neuropsychopharmacology* 47:3–19.
70. Wallis JD (2011): Cross-species studies of orbitofrontal cortex and value-based decision-making. *Nat Neurosci* 15:13–19.
71. Heilbronner SR, Rodríguez-Romaguera J, Quirk GJ, Groenewegen HJ, Haber SN (2016): Circuit-based corticostriatal homologies between rat and primate. *Biol Psychiatry* 80:509–521.
72. Vogt BA, Paxinos G (2014): Cytoarchitecture of mouse and rat cingulate cortex with human homologies. *Brain Struct Funct* 219:185–192.
73. Bauernfeind AL, de Sousa AA, Avasthi T, Dobson SD, Raghanti MA, Lewandowski AH, *et al.* (2013): A volumetric comparison of the insular cortex and its subregions in primates. *J Hum Evol* 64:263–279.
74. Monosov IE, Rushworth MFS (2022): Interactions between ventrolateral prefrontal and anterior cingulate cortex during learning and behavioural change. *Neuropsychopharmacology* 47:196–210.
75. Janes AC, Farmer S, Peechatka AL, de B Frederick B, Lukas SE (2015): Insula-dorsal anterior cingulate cortex coupling is associated with enhanced brain reactivity to smoking cues. *Neuropsychopharmacology* 40:1561–1568.
76. Foa EB, Liebowitz MR, Kozak MJ, Davies S, Campeas R, Franklin ME, *et al.* (2005): Randomized, placebo-controlled trial of exposure and ritual prevention, clomipramine, and their combination in the treatment of obsessive-compulsive disorder. *Am J Psychiatry* 162:151–161.
77. Simpson HB, Foa EB, Liebowitz MR, Ledley DR, Huppert JD, Cahill S, *et al.* (2008): A randomized, controlled trial of cognitive-behavioral therapy for augmenting pharmacotherapy in obsessive-compulsive disorder. *Am J Psychiatry* 165:621–630.
78. Hezel DM, Simpson HB (2019): Exposure and response prevention for obsessive-compulsive disorder: A review and new directions. *Indian J Psychiatry* 61(suppl 1):S85–S92.
79. Seo HJ, Jung YE, Lim HK, Um YH, Lee CU, Chae JH (2016): Adjunctive low-frequency repetitive transcranial magnetic stimulation over the right dorsolateral prefrontal cortex in patients with treatment-resistant obsessive-compulsive disorder: A randomized controlled trial. *Clin Psychopharmacol Neurosci* 14:153–160.
80. Nauczyciel C, Le Jeune F, Naudet F, Douabin S, Esquevin A, Vérin M, *et al.* (2014): Repetitive transcranial magnetic stimulation over the orbitofrontal cortex for obsessive-compulsive disorder: A double-blind, crossover study. *Transl Psychiatry* 4:e436.
81. Brunelin J, Mondino M, Bation R, Palm U, Saoud M, Poulet E (2018): Transcranial direct current stimulation for obsessive-compulsive disorder: A systematic review. *Brain Sci* 8:37.
82. Dinn WM, Aycicegi-Dinn A, Göral F, Karamursel S, Yildirim EA, Hacıoglu-Yildirim M, *et al.* (2016): Treatment-resistant obsessive-compulsive disorder: Insights from an open trial of transcranial direct current stimulation (tDCS) to design a RCT. *Neurol Psychiatry Brain Res* 22:146–154.
83. Palm U, Leitner B, Kirsch B, Behler N, Kumpf U, Wulf L, *et al.* (2017): Prefrontal tDCS and sertraline in obsessive compulsive disorder: A case report and review of the literature. *Neurocase* 23:173–177.